Preparation of Manganese Phthalocyanine Nanoparticles by Laser Ablation in Liquid and Application to Bioimaging

Yuchun Wang and Hiroyuki Wada

Tokyo Institute of Technology, Japan
4259 Nagatsuta-cho, Midori-ku, Yokohama, Kanagawa 226-8503 Japan
**Corresponding author's e-mail: wada.h.ac@m.titech.ac.jp*

In this study, nanoparticles of manganese phthalocyanine (MnPc) were synthesized through laser ablation in liquid. The MnPc powder was dispersed in deionized water using sonification, and the resulting suspension was irradiated with a Nd:YAG laser. The synthesized nanoparticles were characterized using various techniques including Scanning Electron Microscope (SEM), Dynamic Light Scattering (DLS), Ultraviolet-visible spectroscopy (UV-Vis), and zeta potential analysis. The SEM analysis revealed that the morphology of the nanoparticles was predominantly spherical particles. The DLS measurements showed that the secondary particle sizes decreased as the laser fluence increased. The UV-Vis spectroscopy results indicated an increase in absorbance at low laser fluence, followed by a decrease at high laser fluence. Additionally, the zeta potential analysis confirmed the dispersion stability of the nanoparticles. The photoacoustic signal generated by the nanoparticles exhibited an increase at low laser fluence and a decrease at high laser fluence. These results demonstrate the successful synthesis of MnPc nanoparticles using laser ablation in liquid. The obtained nanoparticles exhibited desirable morphological characteristics and showed potential for enhancing photoacoustic signals.
DOI: 10.2961/jlmn.2023.02.2004
Keywords: manganese phthalocyanine, nanoparticle, laser-ablation in liquid, photoacoustic imaging, contrast agent

1. Introduction

The field of medical imaging has witnessed remarkable advancements in recent years, enabling non-invasive visualization and characterization of biological tissues and structures. Among the emerging imaging techniques, photoacoustic imaging has gained substantial attention for its unique ability to combine the strengths of both ultrasound and optical imaging modalities. [1] This modality has demonstrated great potential in a wide range of applications, including tumor detection, functional brain imaging, vascular imaging, and monitoring of therapeutic interventions. [1,2]

This technique is based on the photoacoustic effect, which was discovered by Alexander Graham Bell in 1880, in which the absorption of light by a material generates acoustic waves. [3] This effect is based on the principle of thermoelastic expansion, where the absorbed light energy causes rapid heating and subsequent expansion of the material, resulting in the emission of detectable acoustic waves. [4] Photoacoustic imaging offers exceptional spatial resolution and deep tissue penetration, surpassing the limitations of traditional optical imaging methods. [5,6] In photoacoustic imaging, a short laser pulse is delivered to the tissue of interest, where it is absorbed, and this absorption leads to the rapid generation of localized thermal expansion and subsequent acoustic wave, which is detected by ultrasound transducers and used to reconstruct high-resolution images. [7-9]

To maximize the performance and versatility of photoacoustic imaging, the development of suitable contrast agents has become a key focus of research. Contrast agents enhance the specificity and sensitivity of imaging by selectively targeting tissues or structures of interest and providing a stronger photoacoustic signal. These agents should possess favorable optical properties, high photostability, biocompatibility, and the ability to accumulate in the target region for improved contrast. [10,11]

Among the various contrast agents explored for photoacoustic imaging, manganese phthalocyanine has emerged as a promising candidate. Manganese phthalocyanine is a synthetic compound with a unique macrocyclic structure consisting of four isoindole units linked by nitrogen atoms. They exhibit exceptional optical properties, including strong absorption in the near-infrared (NIR) region, which aligns well with the optimal window for tissue imaging. [12,13] NIR is preferred for photoacoustic imaging due to its ability to penetrate living tissue with minimal attenuation. Wavelengths below 600 nm are absorbed by components like hemoglobin, and wavelengths above 1300 nm are strongly absorbed by water, limiting penetration depth. [14,15] The NIR region (approximately 650 nm to 1100 nm) falls within the "optical window," minimizing absorption and scattering in tissue. NIR light can penetrate tissues effectively, enabling non-invasive imaging of deeper structures and facilitating functional studies. [16] Additionally, phthalocyanines offer excellent photostability, enabling

prolonged imaging sessions without degradation or loss of contrast. [17]

Efficient synthesis and formulation of phthalocyanine nanoparticles are crucial for their effective utilization as contrast agents in photoacoustic imaging. Nanoparticles provide several advantages over bulk materials, such as increased surface area, improved stability, and enhanced cellular uptake. [18] Various methods have been explored for the synthesis of phthalocyanine nanoparticles, including chemical synthesis, self-assembly, and precipitation techniques. However, these conventional methods often suffer from limitations such as complex procedures, low yields, and challenges in controlling the size and stability of the nanoparticles. [19,20] Wu et al. synthesized NIR-absorbing phthalocyanine-based nanodots (ZnPc-NDs) using a facile method, yielding nanoparticles with an average diameter of approximately 80 nm. [21] Nitschke et al. produced phthalocyanine nanoparticles with a particle size of 70 nm by "microwave method".[22] Additionally, solvent-stabilized nanoparticles of photoconductive MPcs with sizes below 10 nm were synthesized by Wang et al. [23] Laser irradiation of copper phthalocyanine tetrasulfonate (CuPcTs) microcrystals in specific solvents yielded CuPcTs nanoparticles ranging from 15 to 112 nm in diameter was achieved by Leonard et al. [24] The various methods for metal phthalocyanine (MP) nanoparticle synthesis have revealed that they all achieve desirable particle sizes. However, some of these methods have drawbacks, such as the use of toxic solvents or surfactants, and non-spherical particles. Laser ablation in liquid has emerged as a versatile technique for nanoparticle fabrication, offering precise control over size, and morphology. [25-30] By employing a laser pulse to ablate a target material immersed in a liquid medium, nanoparticles are formed through rapid heating. This technique offers several advantages, including simplicity, purity, and the ability to obtain nanoparticles without the need for additional stabilizers or surfactants. Laser ablation in liquid method utilizes water as a safe solvent for both fabrication and potential application in the human body. Additionally, this method produces spherical-shaped nanoparticles, which are highly advantageous for biological applications. These features make laser ablation in liquid a promising and attractive approach for preparing nanoparticles with excellent potential for biomedical applications.

Nonlinear optical nanoparticles have gained significant interest due to their unique optical properties and potential applications in photonics and optoelectronics. Various materials, including metals, metal oxide and organic compounds, have been investigated for their nonlinear optical properties using laser ablation. By tailoring the composition and morphology of these nanoparticles, their nonlinear responses can be fine-tuned for applications such as optical imaging.[31,32]

This paper presents a novel method for synthesizing phthalocyanine nanoparticles. Phthalocyanine nanoparticles were prepared by laser ablation in liquid and characterized for their potential as contrast agents for photoacoustic imaging. The prepared nanoparticles were observed using scanning electron microscopy (SEM) to assess their morphology. The particle size and size distribution were determined using dynamic light scattering (DLS) analysis. The zeta potential was measured using zeta potential analysis. The chemical structure of the nanoparticles was evaluated through Attenuated Total Reflectance (ATR) spectroscopy, while the absorption spectrum was measured using an ultraviolet-visible (UV-vis) spectrophotometer. Finally, photoacoustic imaging experiments were performed using a photoacoustic imaging apparatus with a light-emitting diode (LED) as the light source.

2. Experimental

In this experiment, a colloidal solution of manganese phthalocyanine was prepared using the laser-ablation method. Initially, 2 mg of manganese phthalocyanine powder (Sigma-Aldrich) was placed in a square glass bottle, followed by the addition of 20 ml of deionized (DI) water. To disperse the powder, the mixture was subjected to sonication for 10 minutes. Subsequently, the suspension of manganese phthalocyanine was irradiated by a laser beam emitted by a Nd:YAG laser (Spectron Laser Systems SL8585G, SHG) with a wavelength of 532 nm and a pulse width of 13 ns. The average laser fluence was calculated based on the pulse energy and then adjusted using neutral density (ND) filters with transmittance levels of 70%, 50%, and 25%. During the laser irradiation process, the suspension was irradiated for 30 min while it was stirred with a magnetic stirrer. An unfocused laser beam was employed for this experiment.

Following the irradiation, the resulting colloidal solution was deposited onto a Cu grid and allowed to dry in preparation for observation using scanning electron microscopy (SEM) (Hitachi High-Technologies S-4800). To determine the average particle size and particle size distribution, dynamic light scattering (DLS) was performed (Sysmex Zetasizer Nano). The same equipment was employed to measure the zeta potential. The absorption spectrum of the nanoparticles was determined using an ultraviolet-visible-near-infrared (UV-vis-NIR) spectrophotometer (Jasco V-670). To evaluate the chemical structure of manganese phthalocyanine nanoparticles, Attenuated Total Reflectance (ATR) spectroscopy was conducted (IRPrestige-21, Shimazu). Moreover, photoacoustic imaging was performed using a specialized apparatus equipped with a light-emitting diode (LED) as the light source (PreXion PreXionLED AcousticX). The LED emitted light with a wavelength of 618 nm. Imaging was conducted by irradiating the sample, suspended in DI water, with the LED light within a tube. The generated photoacoustic signals were then detected.

3. Result and Discussion

Figure 1 showed the SEM images of (a) raw material and the prepared nanoparticles at the laser fluence of (b) 75, (c) 150, (d) 210, and (e) 300 mJ/cm^2. The raw material had a rod-like shape, with a particle size of several tens of micrometers in length and a few micrometers in width. And the size of prepared nanoparticles was ranging from 150 to 200 nm, and the size was mostly spherical.

In laser ablation in liquid, the laser beam interacts with the target material, leading to the fragmentation or melting of the material depending on the laser energy used. When a relatively high-energy laser beam is employed, the raw material undergoes fragmentation, resulting in a change in the size of the particles. Alternatively, when the laser ener-

gy is relatively lower, the particles experience melting rather than fragmentation. As the molten material cools down, spherical particles form due to the surface tension forces acting on the material. Spherical nanoparticles are advantageous for various applications due to their uniformity and enhanced stability. [33]

The Gaussian intensity profile describes how the energy is distributed across the beam, with higher energy concentrated at the center and decreasing towards the edges. [34] This energy distribution affects the spatial distribution of energy absorption in the target material. As the laser beam interacts with the material, the higher energy at the center induces fragmentation of the particles, resulting in the formation of smaller nanoparticle fragments. The energy absorbed by the particles at the edges is sufficient to melt the material rather than cause fragmentation.

When nanoparticles are introduced into the bloodstream, those exceeding 500 nm are typically captured by Kupffer cells in the liver, [35] while particles smaller than 20 nm are eliminated through the kidneys. [36] The Enhanced Permeability and Retention (EPR) effect, [36-37] observed in tumor tissues, is characterized by newly formed blood vessels with irregular shapes and larger gaps (around 300 nm to 700 nm) compared to normal vessels. Exploiting these gaps, small particles can infiltrate the tumor tissue through blood vessels. Moreover, due to the limited presence of well-developed lymphatic vessels in tumors, particles tend to accumulate within the tumor site. [38] Generally, nanoparticles ranging from 20 nm to 200 nm exhibit the highest propensity for accumulation in tumors, making them suitable candidates for targeted imaging purposes.

In Figure 2, the size distribution and secondary particle size of the prepared samples were examined using DLS at various laser fluences. Increasing the laser fluence from 75 to 300 mJ/cm^2 led to a reduction in secondary particle sizes. At a laser fluence of 75 mJ/cm^2, the particle size exceeded 200 nm. For the samples synthesized with higher laser fluences from 150 to 300 mJ/cm^2, the particle sizes ranged between 20 and 200 nm, which is within the desired range for contrast agents. These observations highlight the critical role of laser fluence in controlling the size of the synthesized nanoparticles. By adjusting the laser fluence, it is possible to tailor the particle sizes to meet the specific requirements of contrast agents.

The observed decrease in particle size can be attributed to a photothermal ablation mechanism. [39-43] When the raw-material powder is irradiated by a laser beam, its temperature rises rapidly, leading to the development of inner stress within the material. This stress, in turn, causes the powder to fragment into smaller particles. This fragmentation process continues, generating particles of reduced size.

The amount of energy absorbed by the particles is directly proportional to the laser fluence. [44] As the laser fluence increases, a greater amount of energy is transferred to heat, facilitating the fragmentation of the material into smaller particles. However, it is worth noting that the particle size reduction becomes less significant when the laser fluence increases from 150 to 300 mJ/cm^2. This can be attributed to the fact that as the particle size decreases, the fragmentation process gradually slows down. The absorption of energy from the laser beam is determined by the cross-sectional area of the particles. Consequently, as the particle size decreases, the amount of absorbed energy decreases as well.

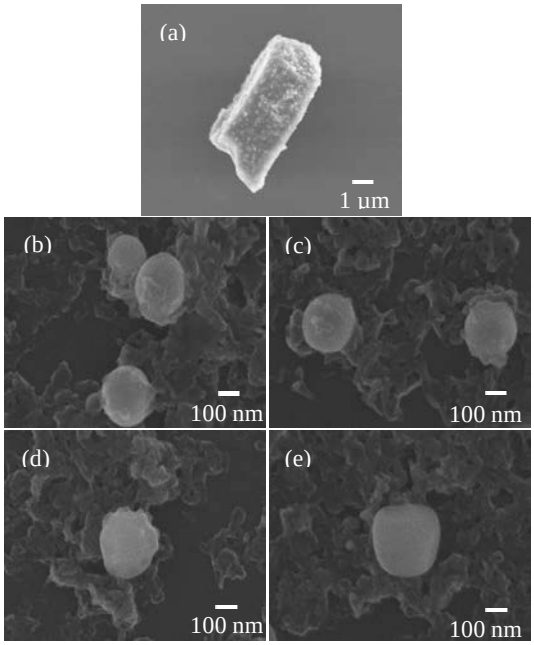

Fig. 1 SEM images of (a) raw material and prepared nanoparticles at the laser fluence of (b) 75, (c) 150, (d) 210, (e) 300 mJ/ cm^2.

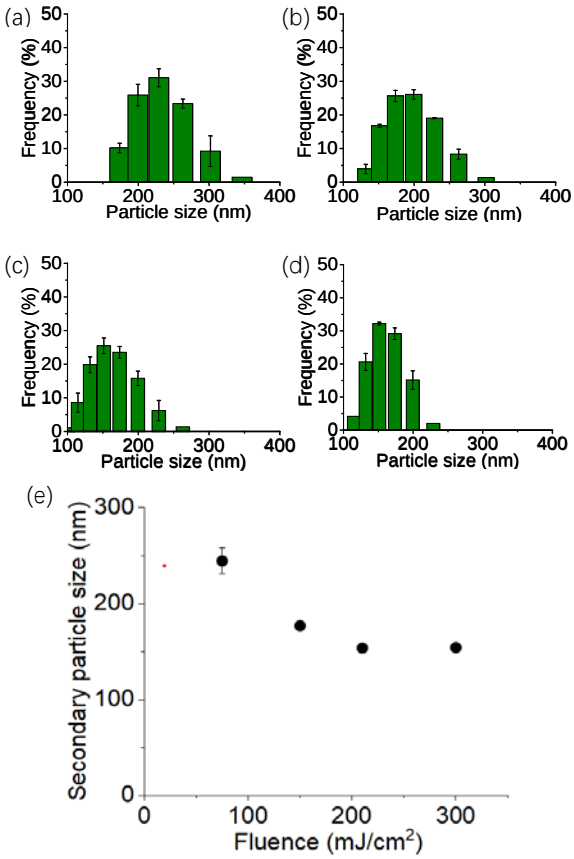

Fig. 2 The size distribution of nanoparticles prepared at the laser fluence of (a) 75, (b) 150, (c) 210, (d) 300 mJ/cm^2, and (e) secondary particle size at varying laser fluence.

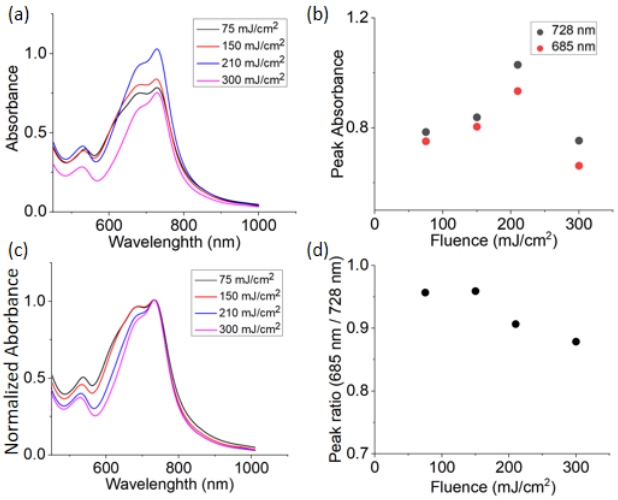

Fig. 3 (a) Absorption spectra of nanoparticle-dispersed solution at varying laser fluence (b) Peak absorbance at 685 nm and 728 nm as a function of laser fluence (c) Normalized absorption spectra of nanoparticle-dispersed solution at varying laser fluence (d) Peak ratio of 685 nm and 728 nm as a function of laser fluence.

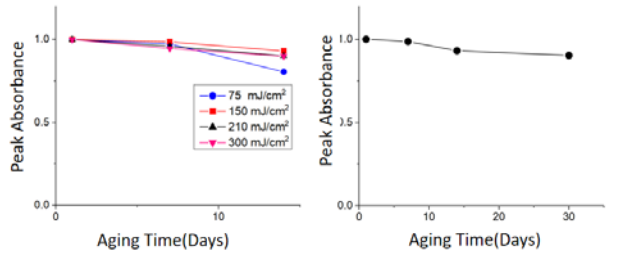

Fig. 4 (a) Peak intensity of absorbance as a function of aging time at each laser fluence (b) Peak intensity of absorbance as a function of aging time at 150 mJ/cm^2.

Moreover, the decrease in particle size results in an increase in the specific surface area of the particles. This increased surface area enhances the thermal diffusion rate between the particles and the surrounding solvent. [41] Consequently, the heat generated during laser irradiation is more efficiently dissipated, further influencing the particle fragmentation process. As the particle size becomes finer, the fragmentation process eventually reaches a point where it is effectively halted.

Figure 3(a) presents the absorbance of the nanoparticles as a function of wavelength at different laser fluences. The absorption spectra exhibit two prominent peaks in the Q band region, approximately at 685 nm and 728 nm, falling within the optical window range. Figure 3(b) illustrates the peak absorbance at these wavelengths as a function of laser fluence. The peak intensity initially increases with increasing laser fluence up to 210 mJ/cm^2 but subsequently decreases when the fluence is further increased to 300 mJ/cm^2.

The change in absorbance can be attributed to multiple factors. One potential explanation for the increase in absorbance with increasing laser fluence is the higher number of prepared nanoparticles. As the fluence increases, more laser energy is available for the ablation process, resulting in the generation of a larger quantity of nanoparticles. The increased number of nanoparticles leads to a greater overall absorbance signal. As for the decrease in absorbance when the fluence is increased to 300 mJ/cm^2, it is suggested that the nanosizing effect and the increased number of nanoparticles could promote the agglomeration of particles, thus reducing the effective number of individual nanoparticles and cause a decrease in overall absorbance.

Additionally, changes in the crystal structure of MnPc nanoparticles could also play a role. MnPc can exist in two crystal forms: α-type, which exhibits higher absorption at 685 nm, and β-type, which shows higher absorption at 728 nm. In Figure 3(c), the UV-vis spectrum is normalized at 728 nm, revealing that the peak absorbance at 685 nm decreases as the laser fluence increases. Furthermore, Figure 3(d) displays the peak ratio of absorbance at 685 nm and 728 nm. The decreasing peak absorbance ratio at 685 nm with increasing laser fluence further supports the notion of crystal structure transformation from α to β. The heat generated during laser irradiation can induce structural changes in the nanoparticles, subsequently altering the absorbance properties of the MnPc nanoparticles. [45, 46]

The stability of colloidal dispersions is a crucial aspect of their practical application. Therefore, evaluating the long-term stability of the prepared samples is of great importance. In this experiment, the absorbance of the aged solution was monitored over a period of 1, 7, 15, and 30 days to assess its stability. Over time, as nanoparticles agglomerate and precipitate, the absorbance of the sample gradually decreases.

Figure 4(a) illustrates the peak intensity of absorbance at each laser fluence after aging the solution for 1, 7, and 15 days. Notably, only the sample prepared using a laser fluence of 75 mJ/cm^2 exhibited a decrease in peak absorbance by over 20%. In contrast, the sample prepared under a laser fluence of 150 mJ/cm^2 demonstrated higher stability. This observation suggests that the laser fluence used during synthesis significantly impacts the stability of the colloidal dispersion.

Furthermore, Figure 4(b) presents the peak intensity of absorbance specifically for the sample prepared using a laser fluence of 150 mJ/cm^2 after aging for 30 days. The results indicate that the sample exhibits relatively high stability even after an extended aging period. The results highlight the significance of selecting an appropriate laser fluence to ensure desirable stability characteristics, with the sample prepared under a laser fluence of 150 mJ/cm^2 demonstrating superior stability.

The findings from the analysis of zeta potential further support and validate the results obtained. In accordance with the DLVO theory, [47] which governs the stability of colloidal dispersions, higher zeta potentials are indicative of increased stability. Figure 5 provides empirical evidence, clearly illustrating that the sample prepared using a laser fluence of 150 mJ/cm^2 exhibited the highest zeta potential among all the samples tested.

Zeta potential is a critical parameter that reflects the electrostatic repulsion between particles in a colloidal system. A higher zeta potential signifies a greater degree of electrostatic stabilization, preventing particle aggregation and ensuring long-term stability. In this case, the sample synthesized with a laser fluence of 150 mJ/cm^2 displayed the highest zeta potential, suggesting stronger repulsive

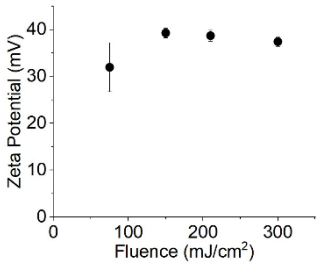

Fig. 5 Zeta potential as a function of laser fluence.

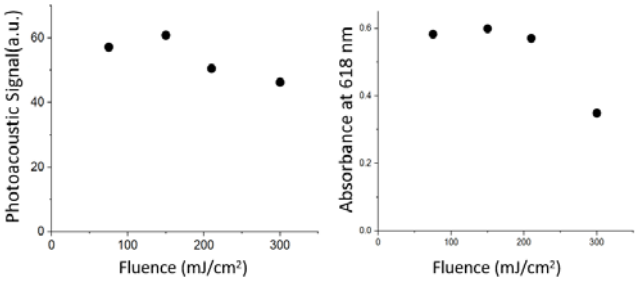

Fig. 6 (a) Photoacoustic signal as a function of laser fluence (b) Absorbance of nanoparticle dispersed solution at 618 nm as a function of laser fluence.

forces between the nanoparticles and enhanced stability within the dispersion.

Figure 6 illustrates the relationship between the photoacoustic signal, measured at a specific wavelength of 618 nm, and the laser fluence. The pressure of the photoacoustic wave P_0 can be expressed by the following equation: [48, 49]

$$P_0 = \left(\frac{\beta c^2}{C_p}\right)\mu_a F = \Gamma \mu_a F$$

where β is the volume-expansion coefficient, c is the sound speed, Γ is the Grüneisen coefficient, μ_a is the absorption coefficient, and F represents the irradiation fluence. And $\beta c^2/C_p$ is the Grüneisen coefficient expressed by Γ.

The Grüneisen coefficient plays a crucial role in quantifying the efficiency of converting light into thermoelastic waves in photoacoustic imaging. The pressure generated by the photoacoustic wave is directly proportional to both the energy of the incident light absorbed by the photoacoustic absorber and the absorption coefficient of the absorber material.

In the present study, as the laser fluence increased from 75 mJ/cm^2 to 150 mJ/cm^2, the photoacoustic signal exhibited a corresponding increase, and when the fluence was further increased from 150 to 300 mJ/cm^2 the photoacoustic signal demonstrated a decline. This trend mirrors the behavior observed in the absorbance measurements at 618 nm, suggesting a correlation between the two phenomena. The variation in the molar absorption coefficient resulting from changes in nanoparticle formation efficiency can account for this observed trend. As the laser fluence changes, the formation efficiency of nanoparticles may be influenced, leading to changes in their absorption coefficient.

In Figure 7, the attenuated total reflectance (ATR) spectrum of both the manganese phthalocyanine raw material and the nanoparticles prepared at different laser fluences is presented. Upon laser irradiation, notable changes are observed in the spectrum, with the emergence of several new peaks. Specifically, new peaks appear in the spectral range of 3050-2900 cm^{-1}, 1666 cm^{-1}, and 1392 cm^{-1}, indicating

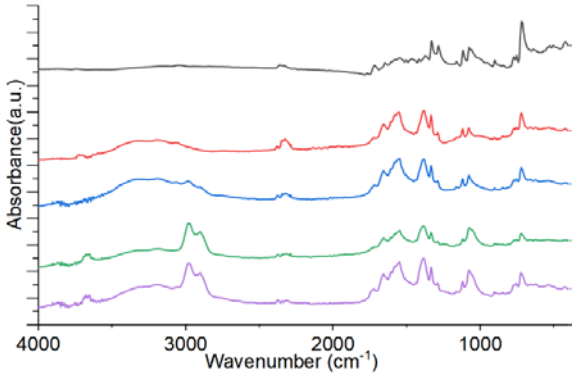

Fig. 7 ATR spectrum of manganese phthalocyanine (a) raw material and nanoparticles prepared at the laser fluence of (b) 75, (c) 150, (d) 210, (e) 300

the formation of carboxylate groups on the surface of the nanoparticles. [50] The presence of these peaks suggests the involvement of oxidation processes triggered by the laser beam. As the laser irradiation interacts with the liquid medium, reactive species are generated, which can induce chemical modifications on the surface of the particles.

The ATR spectrum provides valuable evidence of the chemical changes induced by laser irradiation during the nanoparticle synthesis process. These functional groups can influence the particle's surface charge, which might contribute to the change of Zeta potential. [25]

4. Conclusion

Manganese phthalocyanine nanoparticles were successfully prepared by laser ablation in liquid. The nanoparticles exhibited predominantly spherical shapes. The particle sizes were reduced with an increase in laser fluence, resulting in smaller particles. The absorbance of the nanoparticles showed an initial increase at low laser fluence, followed by a decrease at high laser fluence. With increasing laser fluence, the elevated temperatures prompted a transition in the crystal structure of the particles from the α-phase to the β-phase. The UV-vis spectrum and zeta potential measurements indicated that the sample prepared at a laser fluence of 150 mJ/cm^2 exhibited the best dispersion stability. The photoacoustic signal demonstrated a similar trend to the absorbance, with an increase at low laser fluence and a decrease at high laser fluence. This correlation suggests that changes in the molar absorption coefficient may be responsible for the observed photoacoustic signal variations. Additionally, the ATR spectrum analysis revealed the formation of carboxylate groups on the nanoparticles after laser irradiation.

References

[1] S. L. Chen and C. Tian, Vis. Comput. Ind. Biomed. Art., 4, (2021) 6.
[2] P. Guenther, N. Robert, and F. Martin, J. Appl. Phys., 128, (2020) 180907.
[3] A. G. Bell, Am. J. Sci, s3-20, (1880) 305.
[4] K. Wilson, K. Homan, and S. Emelianov, Nat. Commun., 3, (2012) 618.
[5] L. V. Wang and S. Hu, Science, 335, (2012) 1458.

[6] X. L. Dean-Ben, S. Gottschalk, B. M. Larney, S. Shoham, and D. Razansky, Chem. Soc. Rev., 46, (2017) 2158.
[7] M. Erfanzadeh and Q. Zhu, Photoacoustics, 14, (2019) 1.
[8] P. K. Upputuri and M. Pramanik, Biomed. Eng. Lett., 8, (2018) 167.
[9] F. Gao, X. Feng, R. Zhang, S. Liu, R. Ding, R. Kishor, and Y. Zheng, Sci. Rep., 7, (2017) 626.
[10] Q. F, R. Zhu, J. Song, H. Yang, and X. Chen, Adv. Mater., 31, (2019) 1805875.
[11] W. Choi, B. Park, S. Choi, D. Oh, J. Kim, and C. Kim, Chem. Rev., 88, (2023) e202300173.
[12] B. D. Zheng, J. Ye, Y. Y. Huang, and M. T. Xiao, Biomater. Sci., 9, (2021) 7811.
[13] X. Li, E. Y. Park, Y. Kang, N. Kwon, M. Yang, S. Lee, W. J. Kim, C. Kim, and J. Yoon, Angew. Chem. Int. Ed., 132, (2020) 8708.
[14] C. Ash, M. Dubec, K. Donne, and T. Bashford. Lasers. Med. Sci., 32, (2017) 1909.
[15] M. Wheelock, J. Culver, and A. Eggebrecht. Rev. Sci. Instrum., 90, (2019) 051101.
[16] Y. Y. Huang, A. C. H. Chen, and M. Hamblin, SPIE Newsroom (2009).
[17] R. Słota and G. Dyrda, Inorg. Chem., 42, (2003) 5743.
[18] E.Y. Park, D. Oh, S. Park, W. Kim, and C. Kim. Appl. Phys. Lett. Bioeng., 30, (2021) 031510.
[19] W. Borzęcka, A. Domiński, and M. Kowalczuk, Nanomaterials., 11, (2021) 2426.
[20] T. Furuyama, K. Satoh, T. Kushiya, and N. Kobayashi, J. Am. Chem. Soc., 136, (2014) 765.
[21] F. Wu, L.Yue, K. Cheng, J. Chen, K-L. Wong, W-K. Wong, and X. Zhu. ACS Biomater. Sci. Eng., 6, (2020) 5230.
[22] C. Nitschke, S. M. O'Flaherty, M. Kröll, and W. J. Blau. J. Phys. Chem. B., 108, (2004) 1287.
[23] Y. Wang and D. Liang, Adv. Mater., 22 (2010) 1521.
[24] K. Leonard, M. T. Tun, J. Kurawaki, T. Akiyama, and S. Yamada, e-J. Surf. Sci., 6, (2008) 312.
[25] J. Neddersen, G. Chumanov, and T. Cotton, Appl. Spectrosc., 47, (1993) 1959.
[26] A. Fojtik and A. Henglein, Ber. Bunsenges. Phys. Chem., 97, (1993) 252.
[27] D. Zhang, B. Gökce, and S. Barcikowski, Chem. Rev., 117, (2017) 3990.
[28] D. Zhang, Z. Li, and K. Sugioka, J. Phys. Photonics, 3, (2021) 042002.
[29] E. Fazio, B. Gökce, A. De Giacomo, M. Meneghetti, G. Compagnini, M. Tommasini, F. Waag, A. Lucotti, C.G. Zanchi, P.M. Ossi, M. Dell'Aglio, L. D'Urso,M. Condorelli,V. Scardaci, F. Biscaglia, L. Litti, M. Gobbo, G. Gallo, M. Santoro, S. Truss, and F. Neri. Nanomaterials,10, (2020) 2317.
[30] V. Amendola, D. Amans, Y. Ishikawa, N. Koshizaki, S. Scirè, G. Compagnini, S. Reichenberger, and S. Barcikowski. Chem. Eur. J., 26 (2020) 9206.
[31] L. W. Chen and M. H. Hong. Opto-Electron Sci., 1, (2022) 210007.
[32] Y. J. Jin, L. W. Chen, M. X. Wu, X. Z. Lu, R. Zhou, and M. H. Hong, Opt. Mater., 6, (2016) 1114.
[33] Y. Ishikawa, T. Tsuji, S. Sakaki, and N. Koshizaki, Prog. Mater. Sci., 131, (2023) 101004.
[34] Acherjee and Bappa. J. Manuf. Process., 60, (2020) 227.
[35] A. Schadlich, H. Caysa, T. Mueller, F. Tenambergen, C. Rose, A. Gopferich, J. Kuntsche, and K. Mader, ACS Nano, 5, (2011) 8710.
[36] M. Ohlson, J. Sorensson, and B. Haraldsson, Am. J. Physiol. Renal Physiol., 280, (2001) F396.
[37] Y. Matsumura and H. Maeda, Cancer Res., 46, (1986) 6387.
[38] S. J. Shin, J. R. Beech, and K. A. Kelly, Integr. Biol. (Camb), 5, (2013) 29.
[39] R. Yanagihara, T. Asahi, Y. Ishibashi, O. Odawara, and H. Wada, Jpn. J. Appl. Phys., 57, (2018) 035001.
[40] Y. Hosokawa, M. Yashiro, T. Asahi, and H. M. Masuhara, Proc. SPIE, 4274, (2001) 78.
[41] Y. Tamaki, T. Asahi, and H. Masuhara, Jpn. J. Appl. Phys., 42, (2003) 2725.
[42] T. Sugiyama, S. Ryo, I. Oh, T. Asahi, and H. Masuhara, J. Photochem. Photobiol. A, 207, (2009) 7.
[43] R. Yasukuni, T. Hironaka, and T. Asahi, Jpn. J. Appl. Phys., 49, (2010) 06GJ04.
[44] A. Pyatenko, H. Wang, N. Koshizaki, and T. Tsuji, Laser Photonics Rev., 7, (2013) 596.
[45] S. Yim, S. Heutz, and T. S. Jones, J. Appl. Phys., 91, (2002) 3632.
[46] D. Roy, N. M. Das, N. Shakti, and P. S. Gupta, RSC Adv., 4, (2014) 42514.
[47] S. Bhattacharjee, M. Elimelech, and M. Borkovec, Croatica. Chimca. Acta., 71, (1998) 883.
[48] J. A. Viator, S. L. Jacques, and S. A. Prahl, IEEE J. Quantum Electron., 5, (1999) 989.
[49] M. Xu and L. V. Wang, Rev. Sci. Inst., 77, (2006) 041101.
[50] J-J. Max and C. Chapados, J. Phys. Chem. A, 108, (2004) 3324.

(Received: June 15, 2023, Accepted: August 27, 2023